基于周期性微通道长周期光纤光栅的制备与传感特性研究

孙财 李元君 杨禾儿 潘学鹏 刘善仁 王博 高萌萌 国旗 于永森

Preparation and sensing characteristics of long-period fiber gratings based on periodic microchannels

SUN Cai, LI Yuan-jun, YANG He-er, PAN Xue-peng, LIU Shan-ren, WANG Bo, GAO Meng-meng, GUO Qi, YU Yong-sen

您可能感兴趣的其他文章

Articles you may be interested in

Preparation and sensing characteristics of long-period fiber gratings based on periodic microchannels

SUN Cai, LI Yuan-jun, YANG He-er, PAN Xue-peng, LIU Shan-ren, WANG Bo, GAO Meng-meng,
GUO Qi*, YU Yong-sen*

（*State Key Laboratory of Integrated Optoelectronics*, *College of Electronic Science and Engineering*,

Jilin University, *Changchun* 130012, *China*）

＊ Corresponding author，*E-mail*: *qiguo@jlu.edu.cn*; *yuys@jlu.edu.cn*

Abstract: Long-period fiber gratings have the advantages of small size, corrosion resistance, anti-electro-magnetic interference, and high sensitivity, making them widely used in biomedicine, the power industry, and aerospace. This paper proposes a long-period fiber grating sensor based on periodic microchannels. First, a series of linear structures were etched in the cladding of a single-mode fiber by femtosecond laser micromachining. Then, the laser-modified region was selectively eroded by selective chemical etching to obtain the periodic microchannel structure. Finally, the channels were filled with polydimethylsiloxane (PDMS) to improve the spectral quality. The experimental results show that the sensor has good sensitivity in the measurement of various parameters such as temperature, stress, refractive index, and bending: it has a temperature sensitivity of -55.19 pm/°C, a strain sensitivity of -3.19 pm/με, a maximum refractive index sensitivity of 540.28 nm/RIU, and a bending sensitivity of 2.65 dB/m^{-1}. All of the measurement parameters show good linear responses. The sensor has strong application prospects in the field of precision measurement and sensing.

Key words: long-period fiber gratings; femtosecond laser micromachining; fiber sensors

基于周期性微通道长周期光纤光栅的
制备与传感特性研究

孙　财, 李元君, 杨禾儿, 潘学鹏, 刘善仁, 王　博, 高萌萌, 国　旗*, 于永森*

（吉林大学 电子科学与工程学院 集成光电子学国家重点实验室, 吉林 长春 130012）

摘要: 长周期光纤光栅具有体积小、耐腐蚀、抗电磁干扰和灵敏度高等优点, 使其广泛应用于生物医学、电力工业以及航空航天等领域。本文提出了一种基于周期微通道的长周期光纤光栅传感器。首先通过飞秒激光微加工在单模光纤的包

层中刻蚀出一系直线结构，然后通过湿法腐蚀技术对激光改性区域进行选择性腐蚀以获得周期性微通道结构，最后在通道中填充聚二甲基硅氧烷（PDMS）以改善光谱质量。实验结果表明，该传感器可以进行温度、应力、折射率和弯曲等传感参数测量，具有良好的传感灵敏度。温度灵敏度为−55.19 pm/℃，应变灵敏度为−3.19 pm/με，最大折射率灵敏度为540.28 nm/RIU，弯曲灵敏度为 2.65 dB/m⁻¹，且均表现出良好的线性响应。该传感器在精密测量和传感领域有良好的应用前景。

关　键　词：长周期光纤光栅；飞秒激光微加工；光纤传感器

1　Introduction

Long-period fiber gratings (LPFGs) have long played an important role in such fields as high-temperature sensing and distributed sensing[1-2]. Compared with fiber Bragg gratings, the resonance peaks of LPFGs are more sensitive to different external environments. LPFGs have the advantages of mature fabrication techniques, immunity to electromagnetic interference, and high sensitivity. Therefore, they have been widely applied in strain[3-4], temperature[5-6], bending[7-8], refractive index (RI)[9-11], torsion[12-13], and virus[14] sensing. There are many methods for fabricating LPFGs. The most commonly used of these methods are femtosecond laser inscription[2,15], ultraviolet exposure[16], and CO_2 laser irradiation[17-18]. Femtosecond laser inscription has a robust anti-aging capability and large resonance wavelength depth.

In recent decades, the LPFGs with microchannel[19] and micropore[20] structures obtained by femtosecond laser inscription have been developed rapidly and widely applied in temperature, RI, and curvature sensing. Guo *et al.* proposed an LPFG based on periodic microchannels. First, a femtosecond laser is used to inscribe the periodic linear structures in single-mode fiber (SMF). Then, hydrofluoric acid is used to etch the laser-modified regions to obtain microchannels. This LPFG achieved highly sensitive measurements of environmental RI changes[19]. Lan *et al.* proposed a novel LPFG with internal micropores, which is highly robust. The femtosecond laser was first used to inscribe the periodic linear structures in the core of the SMF, and

then micropores were formed by discharging in the region of the short lines[20]. Gong *et al.* developed a fiber Mach-Zehnder interferometer (MZI) sensor. The MZI was formed by fabricating a hollow ellipsoid in the fiber. The sensor can be used for bending sensing in an extensive curvature range[21]. From the works above, it can be concluded that the LPFG with microchannel and micropore structures exhibits good sensing characteristics and study values.

In this work, a novel LPFG based on periodic microchannels is proposed. The femtosecond laser first inscribes a series of line structures in the SMF cladding. Then, the periodic microchannels are formed by hydrofluoric acid etching of the femtosecond laser direct writing regions. The microchannels are filled with polydimethylsiloxane (PDMS) to obtain a better transmission spectrum. Meanwhile, the length of the grating period is as small as 30 μm. The experimental results show that the temperature sensitivity is −55.19 pm/°C in the range of 26 °C to 90 °C, and the strain sensitivity is −3.19 pm/με in the range of 0 to 1 568 με. In addition, the RI sensitivities are 154.31 nm/RIU in the range of 1.333 to 1.399 and 540.28 nm/RIU in the range of 1.399 to 1.427 5, and the bending sensitivity is 2.65 dB/m⁻¹. This LPFG is low cost, robust, and has potential application value in multi-parameter sensing.

2　Experiment

2.1　Fabrication of LPFG

The experimental equipment of the LPFG fabrication system is shown in Fig. 1. The laser used in the system is the femtosecond laser of the Pharos series (PH1-10 W) manufactured by Light Conver-

sion. The 1 030 nm femtosecond laser is frequency doubled to 515 nm by using β-BaB$_2$O$_4$ (BBO) crystal. The repetition frequency is 10 kHz, and the pulse duration is 230 fs. After the femtolaser has passed through reflectors, a collimated beam, and a dichroic mirror, it is then focused into the fiber cladding by a 60× oil immersion objective (Olympus, NA = 1.42). The fiber is fixed on a three-axis translation platform controlled by a computer, which precisely controls the movement of the fiber. The laser direct writing process can be seen in real time on the computer screen through the charge-coupled device (CCD).
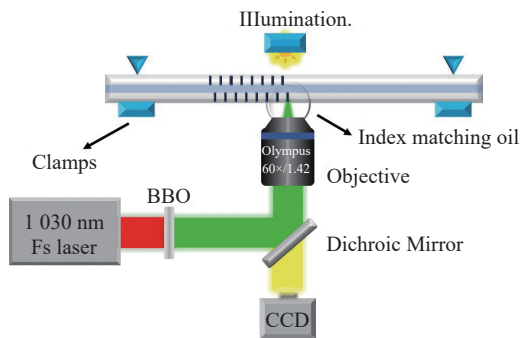

Fig. 1　The LPFG fabrication system

In the experiment, the three-axis translation stage precisely controlled the movement of the fiber, and the computer precisely controlled the laser shutter. As shown in Fig. 2(a), the fiber moved perpendicular to the laser incident direction during fabricating to achieve a linear laser-modified structure. When the laser scanning position was close to the fiber's core, the laser shutter was closed to position the laser modulation region in the fiber's cladding. The laser scan length was approximately 56 μm. After scanning the first laser modulation region, the fiber was axially translated by 30 μm, and the above step was repeated, where the translation distance was the grating period. The LPFG has approximately 166 cycles and a total length of 10 mm.

Then, the microchannel structures were obtained by hydrofluoric acid etching of laser-modified regions. The periodic laser-modified linear fiber was immersed in a 20% hydrofluoric acid solution to achieve selective etching. During the above process, the etching was mainly carried out in the laser-modified region because the corrosion rate in the laser-modified region was more than two hundred times higher than that in the unmodified region[22]. To avoid high insertion loss, it was necessary to accurately control the etching time to ensure that the processed region was completely corroded without eroding into the fiber core. Through many comparative experiments, the best corrosion effect was found to be obtained by controlling the etching time at 20 minutes. At this duration, the spectrum was found to be optimal and there was no high insertion loss. Fig. 2(b) shows the microscopic image of the cladding etched LPFG. The width of the microchannels was approximately 8 μm.
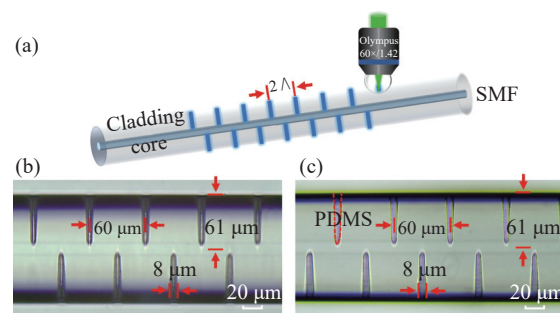

Fig. 2　(a) Schematic diagram of the periodic straight-line laser-modified structure by fs laser direct writing. (b) Microscope image of LPFG after HF etching. (c) Microscope image of LPFG with PDMS filling.

After completing the above steps, the PDMS was filled into the corroded microchannels to improve the spectral quality. The PDMS solution was prepared with a 1:10 ratio of S184-B and S184-A, and then the PDMS was dropped around the microchannels obtained by hydrofluoric acid etching. At the same time, the fiber was placed in the ultrasonic machine so that the PDMS entered the microchannels completely. The PDMS was solidified by a heating stage after completely entering the microchannels. Fig. 2(c) shows the microscopic image of the microchannel after filling the channels with PDMS.

2.2　Sensing Principle

The LPFGs can achieve coupling between the core and cladding modes of the same direction

transmission. According to the coupled mode theory, the resonant wavelength of the LPFG can be expressed as[23-25]:

$$\lambda_m = \left(n_{eff}^{co} - n_{eff}^{cl} \right) \Lambda \quad , \qquad (1)$$

where λ_m is the resonant wavelength, n_{eff}^{co} and n_{eff}^{cl} are the effective refractive index of the core and cladding modes, respectively, and Λ is the grating period.

The resonant wavelength of the LPFG at different temperatures is expressed as[6]:

$$\frac{d\lambda_m}{dT} = \left(\frac{dn_{eff}^{co}}{dT} - \frac{dn_{eff}^{cl}}{dT} \right) \Lambda + \left(n_{eff}^{co} - n_{eff}^{cl} \right) \frac{d\Lambda}{dT}, \quad (2)$$

When the ambient temperature changes, $d\Lambda/dT$ represents the change in grating period caused by the fiber's thermal expansion effect, dn_{eff}^{co}/dT and dn_{eff}^{cl}/dT represent the changes in the effective refractive index of the core and cladding modes caused by the thermal optical effect.

The resonant wavelength of the LPFG under the axial strain ε is expressed as[4]:

$$\frac{d\lambda_m}{d\varepsilon} = \left(\frac{dn_{eff}^{co}}{d\varepsilon} - \frac{dn_{eff}^{cl}}{d\varepsilon} \right) \Lambda + \left(n_{eff}^{co} - n_{eff}^{cl} \right) \frac{d\Lambda}{d\varepsilon}, \quad (3)$$

When the axial strain is applied to the fiber, $dn_{eff}^{co}/d\varepsilon$ and $dn_{eff}^{cl}/d\varepsilon$ present the changes in the effective refractive index of the core and cladding modes caused by the elastic optical effect.

As can be seen from formulas (2) and (3), since the refractive index of PDMS decreases when the temperature and strain increase, the resonant peak moves in the short wavelength direction in the temperature and strain sensing tests.

3　Results and Discussion

After the device preparation was completed, the sensing characteristics of the device were investigated. Fig. 3 shows the initial transmission spectrum of the LPFG through an optical spectrum analyzer (OSA). The OSA is the model AQ6370D produced by Yokogawa. The highest resolution is 0.02 nm.
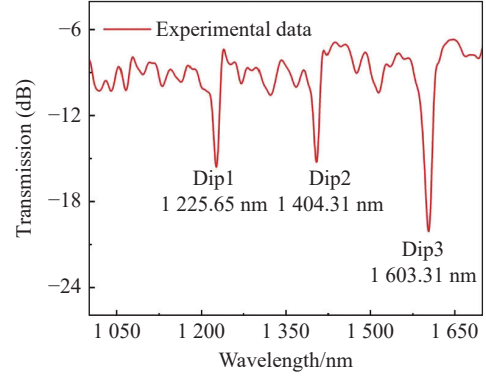

Fig. 3　Initial transmission spectrum of LPFG.

It can be observed from Fig. 3 that three distinct valleys are seen in the initial transmission spectrum in the range of 1 000 nm to 1 700 nm, which are named dip1, dip2, and dip3. The wavelengths of the dips are 1 225.65 nm, 1 404.31 nm, and 1 603.31 nm, respectively. The resonant wave length dip1 was observed in the following tests. Subsequently, a fiber sensing test system was established for temperature, strain, RI, and bending sensing measurements.

3.1　Sensing Test System

Fig. 4 shows the experimental equipment of the sensing test system. During the tests, light originated from the light source and entered the sensing device through the SMF. The SuperK COMPACT supercontinuum light source produced by NKT Photonics was used. It has an output wavelength of 400-2 400 nm and an output power of 110 mW and is a non-polarized light source. The spectral changes during the process of sensing tests were recorded by the OSA.
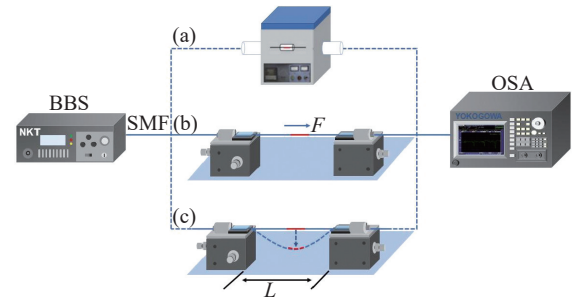

Fig. 4　Schematic diagram of the experimental setup for measuring (a) temperature, (b) strain and (c) bending.

3.2 Temperature Sensing

The spectral response to temperature is first carried out. Fig. 4(a) shows the setup of the temperature test. During the test, it was essential to keep the LPFG straight to avoid spectral changes due to bending. The LPFG was fixed in a tube furnace with a temperature resolution of 0.1 °C. The tube furnace was gradually heated from 26 °C to 90 °C in steps of 10 °C. At each temperature test point, the tube furnace temperature was maintained for sixty minutes to ensure that the environmental temperature of the LPFG had stabilized. The transmission spectra at different temperatures are recorded in Fig. 5(a). It shows that dip1 blue shifts as the temperature increases. Dip1's wavelength values at different temperatures are displayed in Fig. 5(b). The temperature sensitivity is −55.19 pm/°C in the range of 26 °C to 90 °C and the linear fit is 0.993 9.
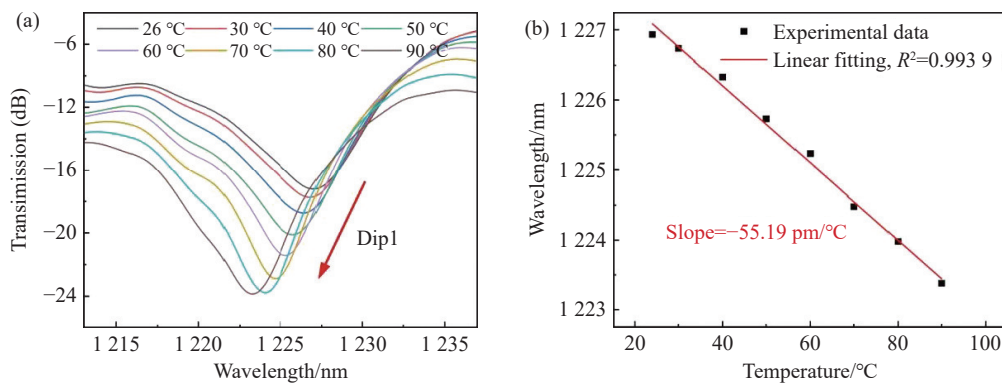

Fig. 5　(a) Evolution of the transmission spectrum at different temperatures; (b) Relationship between the resonance wavelength shift and the temperature.

3.3 Strain Sensing

During the strain sensing test, it was necessary to keep the environmental temperature of the LPFG stable to prevent temperature changes from affecting the strain test results. Fig. 4(b) shows the setup of the strain test. The axial tension was applied to the LPFG using a stress meter for the strain sensing test. The axial strain ε was calculated by the equation:

$$\varepsilon = \frac{F}{\pi r^2 E} \quad , \qquad (4)$$

where F is the axial tension, r is the cladding radius, and E is the Young modulus of the silica fiber. The axial tension was gradually increased from 0 N to 1.4 N in steps of 0.2 N. The transmission spectra at different strains are recorded in Fig. 6(a). It can be observed that dip1 blue shifts as the strain increases. Dip1's wavelength values at different strains are displayed in Fig. 6(b). The strain sensitivity is −3.19 pm/μɛ in the range of 0 to 1 568 μɛ and the linear fit is 0.9983.
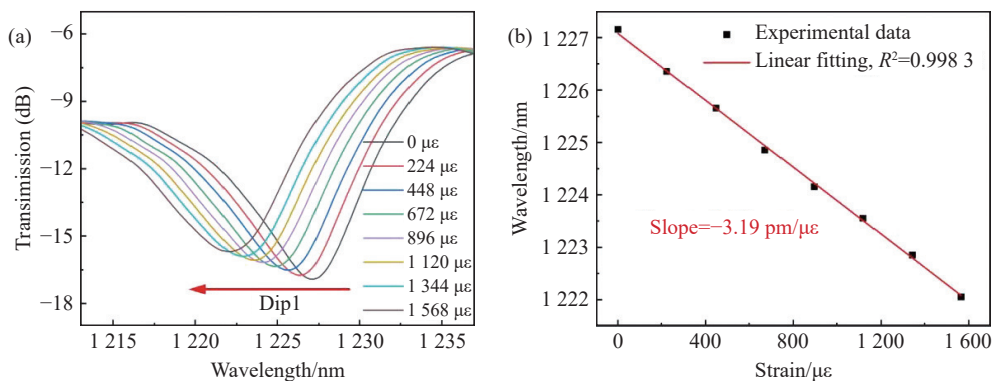

Fig. 6　(a) Evolution of the transmission spectrum at different strains; (b) Relationship between resonance wavelength shift and strain.

3.4　RI Sensing

During the RI sensing test, the LPFG was placed in a hard plastic slot and kept straight. After fixing the LPFG, the RI solutions were injected into the plastic slot until they completely entered the microchannels. There are a total of 14 solutions with different RIs, which were made by mixing glycerin and water in different volume ratios. At each RI test point, the spectrum of the LPFG was recorded after it had stabilized. After recording the spe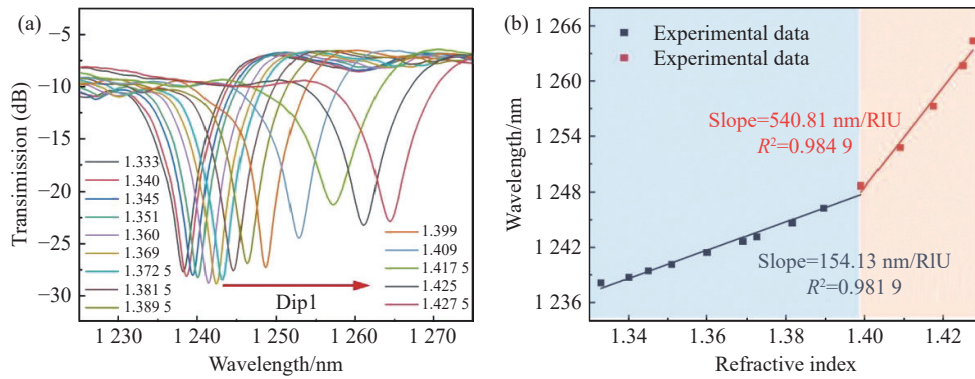ctrum, the LPFG was repeatedly cleaned with deionized water and ethanol and finally dried with compressed air. When the LPFG was recovered, the above process was repeated to measure the other solutions with different RIs. The transmission spectra at different curvatures are recorded in Fig. 7(a). Dip1 red shifts as the RI increases. Dip1's wavelength values at different RIs are displayed in Fig. 7(b). The RI sensitivities are 154.31 nm/RIU in the range of 1.333 to 1.399 and 540.28 nm/RIU in the range of 1.399 to 1.427 5.

Fig. 7　(a) Evolution of the transmission spectrum at different RI solutions; (b) Relationship between resonance wavelength shift and RI.

3.5　Bending Sensing

In the bending sensing test, the LPFG was fixed on two fixtures, as shown in Fig. 4(c). The two fixtures were mounted on an adjustable stage with an accuracy of 0.1 mm. The LPFG was bent by moving the linear motion platform. The curvature (C) was calculated by the following equation[21]:

$$C = 2d/\left(d^2 + L^2\right) , \qquad (5)$$

where L is the initial distance of the two linear motion platforms and d is the movement distance of the two linear motion platforms.

During the sensing test, the curvature of the LPFG gradually increased from 0 to 3 m^{-1} in steps of 0.5 m^{-1}. The transmission spectra at different curvatures are recorded in Fig. 8(a). The intensity of dip1 increases as the curvature increases. Dip1's wavelength values at different curvatures are displayed in Fig. 8(b). The bending sensitivity is -2.65 dB/m^{-1} and the linear fit is 0.9960.
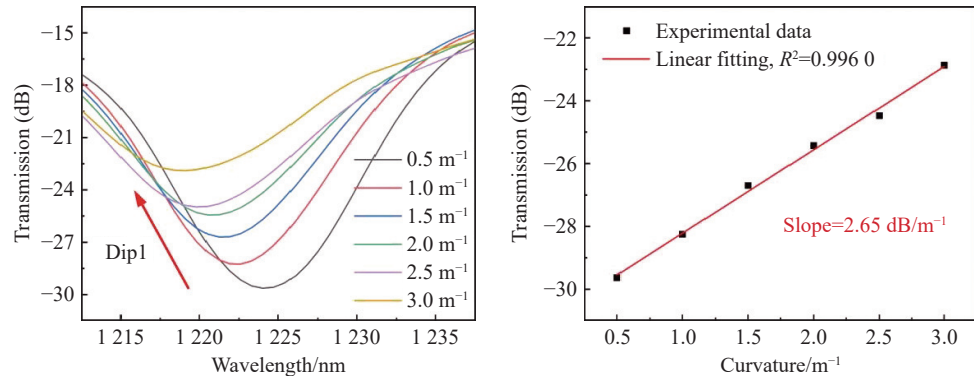

Fig. 8　(a) Evolution of the transmission spectrum at different curvatures; (b) Relationship between resonance intensity shift and curvature.

3.6　Discussion

Finally, Table 1 compares the measurement parameters of sensors with different structures based on LPFG. In recent years, LPFGs with microporous and microchannel structures have been proposed to improve measurement sensitivity. This paper pro-poses a sensor based on periodic microchannels en-graved on SMF cladding. Table 1 shows that com-pared with sensors of other structures, this type of sensor exhibits relatively high sensitivity to temper-ature and can measure multiple parameters separ-ately by controlling variables.

Tab. 1　Comparison of measurement parameters for different types of LPFG

Year	Sensing structure	Temperature sensitivity	Strain sensitivity	RI sensitivity	Bending sensitivity	Reference
2013	Periodic microchannels	9.95 pm/°C	−2.4 pm/με	−391 nm/RIU	−	[19]
2017	Hollow ellipsoid	−	−	−	0.42 dB/m^{-1}	[21]
2022	Inner microholes	13.06 pm/°C	−1.57 pm/με	−	−	[20]
2022	Micro air-channel	12.1 pm/°C	−	587.08 nm/RIU	−	[26]
2023	Taped two-mode fiber and PDMS	−0.412 nm/°C	−12.16 nm/MPa	−	−	[6]
2023	D-shape	45 pm/°C	−	−	17.6 nm/ m^{-1}	[27]
2024	Periodic microchannels on the cladding and PDMS	−55.19 pm/°C	−3.19 pm/με	540.28 nm/RIU	2.65 dB/m^{-1}	This work

4　Conclusion

This paper proposes and introduces a novel type of LPFG based on cladding periodic mi-crochannels. The microchannels were obtained by femtosecond laser direct writing and hydrofluoric acid etching. The PDMS was filled into the perio-dic microchannels of the LPFG to obtain a better transmission spectrum. The LPFG sensor exhibits good sensing sensitivity. It has a temperature sensit-ivity of −55.19 pm/°C, a strain sensitivity of −3.19 pm/με, a maximum RI sensitivity of 540.28 nm/RIU, and a bending sensitivity of 2.65 dB/m^{-1}. As a result of the compactness and high sensitivity of the device, this type of LPFG based on cladding refractive index modulation has potential applications in multi-parameter sensing and precision measurement.

References:

[1]　JIANG J J, HUANG Q Q, MA Y H, *et al.*. Wavelength-tunable L-band mode-locked fiber laser using a long-period fiber grating[J]. *Optics Express*, 2021, 29(17): 26332-26339.

[2]　ZHENG ZH M, YU Y S, ZHANG X Y, *et al.*. Femtosecond laser inscribed small-period long-period fiber gratings with dual-parameter sensing[J]. *IEEE Sensors Journal*, 2018, 18(3): 1100-1103.

[3]　ZHANG Y N, JIANG P, QIAO D, *et al.*. Sensing characteristics of long period grating by writing directly in SMF-28 based on 800 nm femtosecond laser pulses[J]. *Optics & Laser Technology*, 2020, 121: 105839.

[4]　MA Y W, LI X Y, WANG S Y, *et al.*. Highly sensitive strain sensor based on a long-period fiber grating with chain-shaped structure[J]. *Applied Optics*, 2020, 59(33): 10278-10282.

[5]　WANG Q, DU CH, ZHANG J M, *et al.*. Sensitivity-enhanced temperature sensor based on PDMS-coated long period fiber grating[J]. *Optics Communications*, 2016, 377: 89-93.

[6]　DENG L F, JIANG CH, HU CH J, *et al.*. Highly sensitive temperature and gas pressure sensor based on long-period fiber grating inscribed in tapered two-mode fiber and PDMS[J]. *IEEE Sensors Journal*, 2023, 23(14): 15578-15585.

[7]　BARRERA D, MADRIGAL J, SALES S. Long period gratings in multicore optical fibers for directional curvature sensor implementation[J]. *Journal of Lightwave Technology*, 2018, 36(4): 1063-1068.

[8]　ZHOU Q, ZHANG W G, CHEN L, *et al.*. Bending vector sensor based on a sector-shaped long-period grating[J]. *IEEE*

Photonics Technology Letters, 2015, 27（7）: 713-716.

［9］　ESPOSITO F, SRIVASTAVA A, SANSONE L, *et al.*. Sensitivity enhancement in long period gratings by mode transition in uncoated double cladding fibers［J］. *IEEE Sensors Journal*, 2020, 20（1）: 234-241.

［10］　ESPOSITO F, SANSONE L, SRIVASTAVA A, *et al.*. Label-free detection of vitamin D by optical biosensing based on long period fiber grating［J］. *Sensors and Actuators B: Chemical*, 2021, 347: 130637.

［11］　PENG M, LU ZH Q, TANG Y, *et al.*. Femtosecond laser direct writing of long period fiber grating sensor with high refractive index sensitivity［J］. *Optical Fiber Technology*, 2023, 81: 103511.

［12］　REN K L, REN L Y, LIANG J, *et al.*. Online fabrication scheme of helical long-period fiber grating for liquid-level sensing［J］. *Applied Optics*, 2016, 55（34）: 9675-9679.

［13］　DENG H CH, WANG R, JIANG X W, *et al.*. A long period grating sensor based on helical capillary optical fiber［J］. *Journal of Lightwave Technology*, 2021, 39（14）: 4884-4891.

［14］　SHI SH H, WANG X, LUO B B, *et al.*. Avian influenza virus immunosensor based on etched long period fiber grating coated with graphene oxide［J］. *Acta Photonica Sinica*, 2020, 49（1）: 0106002. (in Chinese).

［15］　HINDLE F, FERTEIN E, PRZYGODZKI C, *et al.*. Inscription of long-period gratings in pure silica and germanosilicate fiber cores by femtosecond laser irradiation［J］. *IEEE Photonics Technology Letters*, 2004, 16（8）: 1861-1863.

［16］　NIKOGOSYAN D N. Long-period gratings in a standard telecom fibre fabricated by high-intensity femtosecond UV and near-UV laser pulses［J］. *Measurement Science and Technology*, 2006, 17（5）: 960-967.

［17］　ZHANG L, LIU Y Q, ZHAO Y H, *et al.*. High sensitivity twist sensor based on helical long-period grating written in two-mode fiber［J］. *IEEE Photonics Technology Letters*, 2016, 28（15）: 1629-1632.

［18］　WANG L, ZHANG W G, CHEN L, *et al.*. Torsion sensor based on two cascaded long period fiber gratings fabricated by CO_2 laser pulse irradiation and HF etching technique respectively［J］. *Journal of Modern Optics*, 2017, 64（5）: 541-545.

［19］　GUO J CH, YU Y S, XUE Y, *et al.*. Compact long-period fiber gratings based on periodic microchannels［J］. *IEEE Photonics Technology Letters*, 2013, 25（2）: 111-114.

［20］　LAN F L, WANG D N. Long-period fiber grating based on inner microholes in optical fiber［J］. *Optics Letters*, 2022, 47（1）: 146-149.

［21］　GONG H P, WANG D N, XIONG M L, *et al.*. Optical fiber hollow ellipsoid for directional bend sensing with a large bending range［J］. *Optical Materials Express*, 2017, 7（6）: 1767-1776.

［22］　LAI Y, ZHOU K, ZHANG L, *et al.*. Microchannels in conventional single-mode fibers［J］. *Optics Letters*, 2006, 31（17）: 2559-2561.

［23］　DONG X R, SUN X Y, LI H T, *et al.*. Femtosecond laser fabrication of long period fiber gratings by a transversal-scanning inscription method and the research of its orientational bending characteristics［J］. *Optics & Laser Technology*, 2015, 71: 68-72.

［24］　HECK M, KRÄMER R G, ULLSPERGER T, *et al.*. Efficient long period fiber gratings inscribed with femtosecond pulses and an amplitude mask［J］. *Optics Letters*, 2019, 44（16）: 3980-3983.

［25］　ZHANG SH SH, FANG CH Q, ZHANG CH, *et al.*. A compact ultra-long period fiber grating based on cascading up-tapers［J］. *IEEE Sensors Journal*, 2020, 20（15）: 8552-8558.

［26］　CHAO X W, WANG D N. Ultra-short long-period fiber grating based on a micro air-channel structure［J］. *Optics Letters*, 2022, 47（22）: 5961-5964.

［27］　WANG Q Y, DU CH, ZHAO SH, *et al.*. Curvature sensor based on D-shape fiber long period fiber grating inscribed and polished by CO_2 laser［J］. *Measurement*, 2023, 223: 113665.

Author Biographics：

SUN Cai (1998—), male, from Changchun, Jilin Province, master's degree candidate, obtained a bachelor's degree from Jilin University in 2020, mainly engaged in researching fiber sensing. E-mail: 511082895@qq.com

GUO Qi (1991—), male, from Changchun, Jilin Province, Ph.D., lecturer, obtained Ph.D. from Jilin University in 2022, mainly engaged in researching fiber sensing and laser micro-nano processing. E-mail: qiguo@jlu.edu.cn

YU Yong-sen (1974 —), male, from Changchun, Jilin Province, Ph.D., Professor, Ph.D. Supervisor, obtained Ph.D. from Jilin University in 2005, mainly engaged in researching fiber sensing and laser micro-nano processing. E-mail: yuys@jlu.edu.cn